IEEE Access
Multidisciplinary | Rapid Review | Open Access Journal

Received September 12, 2018, accepted October 14, 2018, date of publication October 23, 2018,
date of current version November 19, 2018.

Digital Object Identifier 10.1109/ACCESS.2018.2877591

Underwater Wide-Area Layered Light Field for Underwater Detection

MENGNAN SUN[1], ZHAORUI GU[2], (Member, IEEE), HAIYONG ZHENG[2], (Member, IEEE), BING ZHENG[2], (Member, IEEE), AND JOHN WATSON[3], (Senior Member, IEEE)

[1]Department of Computer Science and Technology, Ocean University of China, Qingdao 266100, China
[2]Department of Electronic Engineering, Ocean University of China, Qingdao 266100, China
[3]School of Engineering, University of Aberdeen, Aberdeen AB24 3UE, U.K.

Corresponding authors: Haiyong Zheng (zhenghaiyong@ouc.edu.cn) and Bing Zheng (bingzh@ouc.edu.cn)

This work was supported in part by the National Natural Science Foundation of China under Grant 41776113 and Grant 61771440, in part by the Qingdao Municipal Science and Technology Program under Grant 17-1-1-5-jch, and in part by the International S&T Cooperation Program of China under Grant 2012DFG22080.

ABSTRACT In underwater electro-optic detection, image quality can be degraded by the backscattering of light from the illuminated water volume. In practical systems, we tend to simultaneously require a high level of detection distance (DD), field of view (FOV), and depth of field (DOF), but these factors influence each other by the media scattering. To eliminate this restriction, we propose to explore the underwater wide-area layered light field (UWLLF), which classifies the underwater detection area by the DD and distribution characteristics of the light field, to minimize the scattering influence on target detection. Based on the UWLLF, an underwater electro-optic detection system is designed that can achieve the specifications of a 70° FOV and 7.9-fold attenuation length (for the attenuation coefficient 1.43 /m of 532 nm) DD. In addition, with the spatial separation of light energy, the non-detection zone at short ranges is eliminated, yielding an almost full DOF. With these three factors simultaneously improved, the ability of underwater exploration for object detection is enhanced.

INDEX TERMS Underwater technology, optical imaging, object detection, light field, underwater detection.

I. INTRODUCTION

Light energy sharply attenuates when it propagates through water because of absorption and scattering. Unlike the underwater sonar imaging system [1], in underwater electro-optic detection (UEOD) [2]–[8], backscattering can be severe, producing intense levels of image noise at short ranges, while the reflected energy that carries the target information at long distances attenuates to a low level [9]. Both of the above factors contribute to a decrease in the received image contrast, which limits the detection distance and imaging quality of the system [10], [11]. Several technologies based on temporal, spatial, and polarization discrimination, such as line laser scanning (LLS), laser range gating (LRG), optical polarization imaging (OPI), streak tube image lidar (STIL), modulation light imaging (MLI), and structured light imaging (SLI), have been developed to reduce the effects of backscattering. The performance of these systems can be evaluated in terms of detection distance (DD), field of view (FOV), depth of field (DOF), power consumption (PC), and portability, volume and weight (PVW). A typical UEOD system should be designed to see farther, wider, and deeper, making the DD, FOV, and DOF the most desired and required evaluation metrics.

The LLS imaging system, such as SM2000 [12], was designed to suppress both back and forward scattering for a better DD based on spatial discrimination by structuring the illumination field to be highly collimated with a minimal cross section [13], [14], resulting in a narrow instantaneous FOV (IFOV) and poor DOF. The LRG system, known as LUCIE [15], was developed to produce a better DD by temporarily ''gating-out'' much of the backscattering [13], whereas the laser pulse width t constrains the DOF to a small level $ct/2$ (c is the speed of light) with a narrow FOV. The OPI system amplifies the signal from targets whose polarization-difference magnitude is distinct from the background [16], yielding a relatively wide FOV but short DD. The STIL system measures the time of flight of the light from the transmitter to the target and back to collect 3D information [17], [18]. When combined with LRG for underwater detection, it has a similar narrow FOV as LRG. The MLI [19] and SLI [20] techniques were mainly used to obtain the depth information of targets from scattering media, which rarely consider FOV and DOF.

TABLE 1. The performance of different UEOD systems.

Tech.	DD	FOV	DOF
LLS [13]	7 AL	1°×70°	Fair
LRG [15]	6-7 AL	<30°	Fair
OPI [16], [21]	Short	Wide	Good
STIL [18]	5-6 AL	8.5°	Poor
MLI [19]	20 AL†	N.A.	N.A.
SLI [20]	6 AL	N.A.	N.A.

† This is only the simulation result at a specific condition.

Table 1 shows the DD, FOV and DOF performances of different UEOD systems. Because the DOF of the existing UEOD systems is not usually quantitated, a qualitative three-level description (poor, fair and good) of DOF performance is made to evaluate the their DOFs, according to their inherent principles. As shown, the DDs of LLS, LRG and STIL can be up to 7 AL (attenuation length), but their FOVs are limited to 30° and their DOFs are constrained to a small range. A relatively wide FOV and good DOF can be obtained by OPI, but its DD is short. Moreover, the FOV and DOF are not available for MLI and SLI because they are not developed to see wide or deep. In conclusion, current UEOD technologies are mostly designed to see farther with a long DD at the expense of a narrow FOV and poor DOF, and the DD will be short if the purpose is changed for a wide FOV and good DOF because more backscattering noise will enter the receiver. In summary, it is difficult to achieve optimal performance in terms of both DD and FOV/DOF simultaneously. To overcome this limitation, we propose the underwater wide-area layered light field (UWLLF) for underwater detection in this paper.

II. UNDERWATER WIDE-AREA LAYERED LIGHT FIELD

A. DESCRIPTION OF UWLLF

Different light sources can create different light fields of different energy distributions, which produce different DDs in the same water quality. Based on the DD differences of different light fields, the underwater detection area by auxiliary illumination is divided into 5 levels of field (as shown in Figure 1): low-energy inhomogeneous light field (LILF, [0, 3.5 AL]), high-energy collimated light field (HCLF, [3.5 AL, 5.25 AL]), remote diffuse light field (RDLF, [5.25 AL, 7 AL]), pulse power light field (PPLF, [7 AL, 10 AL]), and beyond light field (BLF, [10 AL, ∞]), constituting the underwater wide-area layered light field (UWLLF).

1) LILF: The distance from the receiver is short; thus, the illumination will produce severe backscattering, whereas the common homogeneous low-energy illumination is not strong enough for the imaging of distant areas, which means that the energy of the light field needs to be low and distributed inhomogeneously along the receiver axis [22].
2) HCLF: As the distance increases, a common light source cannot generally meet the illumination requirements in this level. As shown in Figure 1, the divergence angle of some level decreases as it heads far away from the receiver. Therefore, a light source with a good collimation property is necessary to establish the HCLF without "polluting" the adjacent levels, compensating for the loss of attenuation. A collimated and homogeneous energy distribution in HCLF is sufficient due to its small illuminated area.
3) RDLF: Through long-distance propagation, the collimated light becomes floodlit to form a diffuse light field. Additionally, the diffuse light also enlarges the illumination area, which benefits the detection area.
4) PPLF: An extremely high light power is required for a long light attenuation path (>7 AL). According to the sampling and exposure characteristics of CCD imaging, it is known that the light energy for imaging in space does not have to exist all the time. Therefore, the light energy can be condensed into a small time slice, meaning that a pulse power illumination with a high instantaneous power can be employed, corresponding to sampling of CCD, both of which contribute to the temporal discontinuity of the light field.
5) BLF: The area in this level is beyond the detection range of the existing UEOD systems.

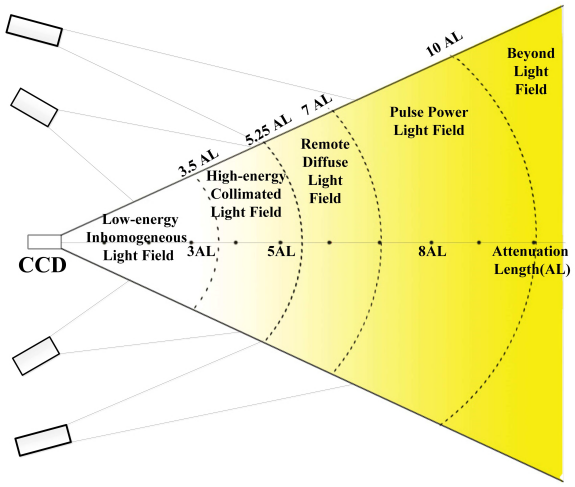

FIGURE 1. Underwater wide-area layered light field.

It is widely accepted that the imaging quality of a UEOD system is associated with the reflected optical energy from the target and the apparent contrast, and they are both determined by the spatial energy distribution. The sensitivity of a CCD and the contrast threshold of the human eye reflect both of these parameters. For an arbitrary point $A(x, y, z)$ in our proposed UWLLF, Equations 1 and 2 show the spatial energy distribution $E_{T_{sum}}(x, y, z)$ and the apparent contrast $C(x, y, z)$, where n refers to the amount levels of UWLLF; E_{Td_i} and E_{Ts_i} represent the received direct and scattered illumination from level i, respectively; and $L_{T_i}(x, y, z)$ and $L_{B_i}(x, y, z)$ are the target luminance and background luminance contributed by

energy level i, respectively.

$$E_{T_{sum}}(x,y,z) = \sum_{i=1}^{n} E_{Td_i}(x,y,z) + \sum_{i=1}^{n} E_{Ts_i}(x,y,z) \quad (1)$$

$$C(x,y,z) = \frac{\sum_{i=1}^{n} L_{T_i}(x,y,z) - \sum_{i=1}^{n} L_{B_i}(x,y,z)}{\sum_{i=1}^{n} L_{B_i}(x,y,z)} \quad (2)$$

UWLLF is proposed to optimize a UEOD system for the purpose of producing a far DD, wide FOV and deep DOF. In UWLLF, $E_{T_{sum}}$ is also transformed to L_{T_i} and L_{B_i} in Equation 2, which is used to calculate $C(x,y,z)$, from which the DD of a UEOD system can be verified. The FOV and DOF determine the size of the backscattering volume represented as $L_{B_i}(x,y,z)$ in Equation 2. It is clear that compressing the FOV and DOF could be helpful for reducing the backscattering (less $L_B(x,y,z)$) to obtain a farther DD (larger $C(x,y,z)$); thus, it is difficult to obtain both a far DD and wide FOV with a deep DOF. Nevertheless, UWLLF is designed with a layered structure of energy distribution to minimize the energy magnitude in the same backscattering volume to reduce $\sum L_{B_i}(x,y,z)$ without reducing the size of the backscattering volume, yielding a far DD with a wide FOV and deep DOF.

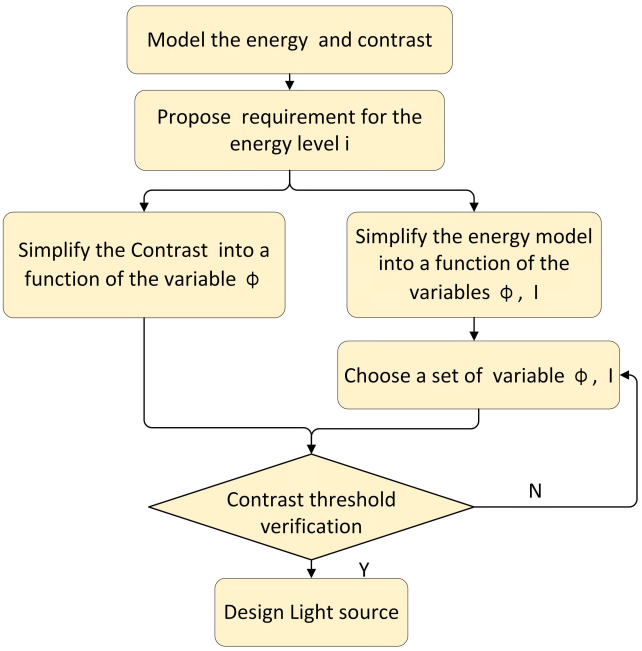

FIGURE 2. Our UWLLF methodology.

B. METHODOLOGY OF UWLLF

The optical energy can be delivered to different levels using different methods, which determines the design of a UWLLF system. Figure 2 illustrates our UWLLF methodology, in which the LILF and HCLF are established in our previous work [22]:

- In the LILF level, a common underwater light source with a slightly collimated ability can be employed, and an appropriate divergence angle is necessary for the inhomogeneous distribution. The area near the CCD in Figure 1, although beyond the area of direct light, could utilize the scattered volume for the illumination.
- A Fresnel lens light source (FLLS) with a special angular distribution can be designed for both HCLF and LILF [22].

Here, we present our procedure for establishing RDLF to illustrate the UWLLF methodology shown in Figure 2.

1) MODEL THE ENERGY AND CONTRAST

The modeling of energy and contrast can be implemented according to Equations 1 and 2. Duntley developed a model to illustrate the energy distribution of direct light and scattered light [23], as shown in Equations 3 and 4, respectively, where E_{Rd} is the portion of direct illuminance and E_{Rs} is the portion of scattered illuminance. Therefore, the energy received by the CCD can be deduced as E_{Rsum} shown in Equation 5.

$$E_{Rd} = \left\{ \exp(-cl - cr) + \frac{lk\exp(-kl - cr)}{4\pi} \times \left(2.5 - 1.5\log\frac{2\pi}{\phi}\right)\left[1 + 7\left(\frac{2\pi}{\phi}\right)^{0.5} \times \exp(-kl)\right]\right\} \frac{\rho\tau I}{4l^2}\left(\frac{D}{f}\right)^2 \quad (3)$$

$$E_{Rs} = \left\{ \exp(-cl - kr) + \frac{lk\exp(-kl - kr)}{4\pi} \times \left(2.5 - 1.5\log\frac{2\pi}{\phi}\right) \times \left[1 + 7\left(\frac{2\pi}{\phi}\right)^{0.5}\exp(-kl)\right]\right\} \times \frac{\rho\tau I\left[rk(1 + 7\sqrt{2}\exp(-kr))\right]}{7.81l^2}\left(\frac{D}{f}\right)^2 \quad (4)$$

$$E_{Rsum} = E_{Rd} + E_{Rs} \quad (5)$$

where I is the light intensity of the light source, ϕ is the beam-divergence angle of the light source, S_0 is the optic-axis distance (from the CCD to the light source), D is the aperture diameter of the CCD, f is the focal length of the CCD lens, c is the attenuation coefficient of water, k is the diffuse attenuation coefficient of water, r is the distance from the target to the CCD, l is the distance from the target to the light source, and ρ is the reflection factor of the target.

The contrast model can be derived from Figure 3. The backscattering luminance $\mathrm{d}L(r)$ from the volume element $\mathrm{d}V$ is derived as:

$$dL(r) = \left\{\frac{I}{l^2}\exp(-cl) + \left(2.5 - 1.5\log\frac{2\pi}{\phi}\right) \times \left[1 + 7\left(\frac{2\pi}{\phi}\right)^{0.5}\exp(-kl)\right]\frac{Ik\exp(-kl)}{4\pi l}\right\} \times \beta(\theta)\exp(-cr)dr \quad (6)$$

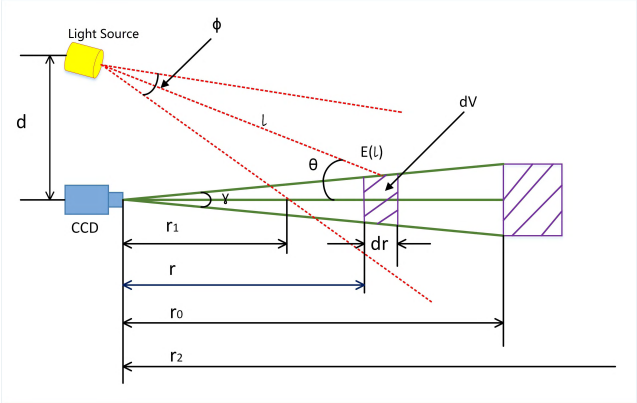

FIGURE 3. The geometrical configuration of the underwater auxiliary illumination system.

According to the definition of the apparent contrast, the apparent contrast of the underwater target is C [24]:

$$C = \frac{L_T + L_P - L_B}{L_B} = \frac{L_T - L(r_0, r_2)}{L(r_1, r_2)} \tag{7}$$

where L_T is the target luminance, L_P is the luminance of the path from the target to the receiver, $L(r_0, r_2)$ is acquired by integrating $\mathrm{d}L(r)$ from r_0 to r_2, and $L(r_1, r_2)$ is obtained by integrating from r_1 to r_2.

TABLE 2. The parameters for the simplification of the energy model and contrast model.

ρ	τ	S_0(m)	D/f	OL(AL)†	k(m^{-1})	r(m)	l(m)
0.6	0.9	1.35	1/1.4	7	c/2.7	5.10	5.28

† $OL = c * r$, which means the optical length. Because the light source in the design is white light, the attenuation coefficient c of natural light is used according to $c = 3.912/visibility$ in this case. $Visibility$ is measured by the Secchi disk [25].

2) SIMPLIFY THE MODEL

The detection area is subsequently set to the RDLF level (7 AL), and Table 2 presents the parameters for simplification. The sensitivity of the CCD (Outland UWC-325) is 0.001 lux, and the contrast limit of the human eye is 0.02. For a high margin of detection, 5-fold of these two thresholds is chosen as the model threshold, corresponding to 0.005 lux and 0.1, respectively. Thus, the energy model is simplified to be a function of ϕ and I, and the contrast model is simplified to be a function of ϕ. As shown in Figure 4, more imaging energy can be acquired with a higher intensity and wider divergence angle of the light source, and the apparent contrast is only related to the divergence angle.

3) CHOOSE A SET OF (ϕ, I) AND PERFORM THE CONTRAST THRESHOLD VERIFICATION

In Figure 4(a), the illuminance of the CCD is plotted with the variables ϕ and I. An arbitrary point above the blue plane is qualified with the energy threshold (0.005 lux), and a set

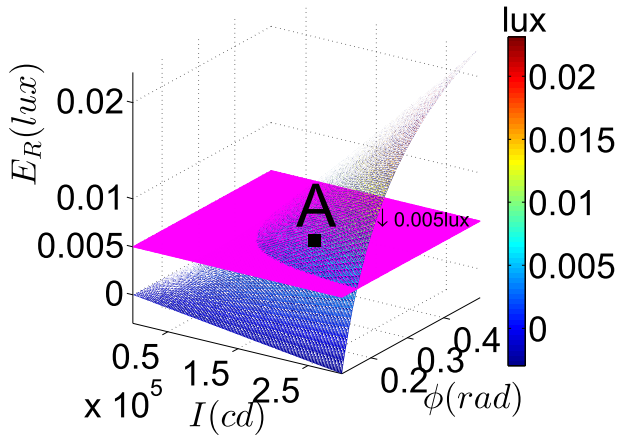

(a)

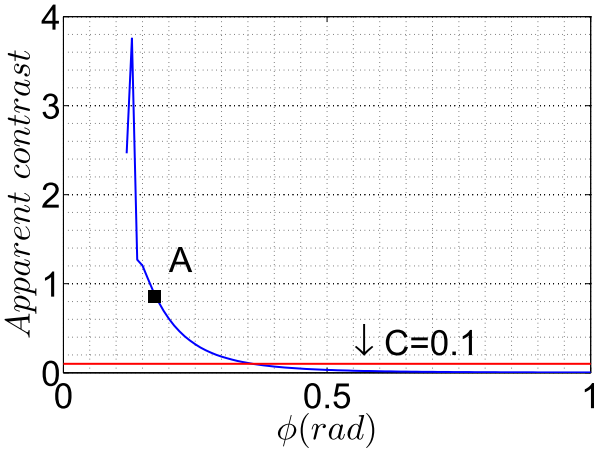

(b)

FIGURE 4. The simplified energy threshold $E_{Rsum}(\phi, I)$ (a) and contrast threshold on specific condition (b).

of (ϕ_A, I_A) (Point A) is selected. Then, ϕ_A is verified by the contrast threshold, as shown in Figure 4(b). Finally, the set (ϕ_A, I_A), meeting both thresholds, is chosen:

$$\phi_A = 0.14\ rad \tag{8}$$

$$I_A = 2.24 \times 10^5\ cd \tag{9}$$

4) DESIGN LIGHT SOURCE

The intensity of 2.24×10^5 cd is divided into 8 light sources (2 arrays) to meet the energy needs (Figure 5(a)). Each array consists of 4 high-power biconvex lens light sources (BLLS), transmitting four collimated beams with a beam-divergence angle of 0.135 rad. Each BLLS contributes a light intensity of $I'_n = 3.28 \times 10^4$ cd (the illuminance distribution is approximately homogeneous in facula using a biconvex len). Therefore, the total tested intensity is:

$$\begin{aligned} I_n &= 8 \times I'_n \\ &= 2.62 \times 10^5\ cd \end{aligned} \tag{10}$$

which indicates that the machined BLLS can meet the design criterion of ϕ_A and I_A.

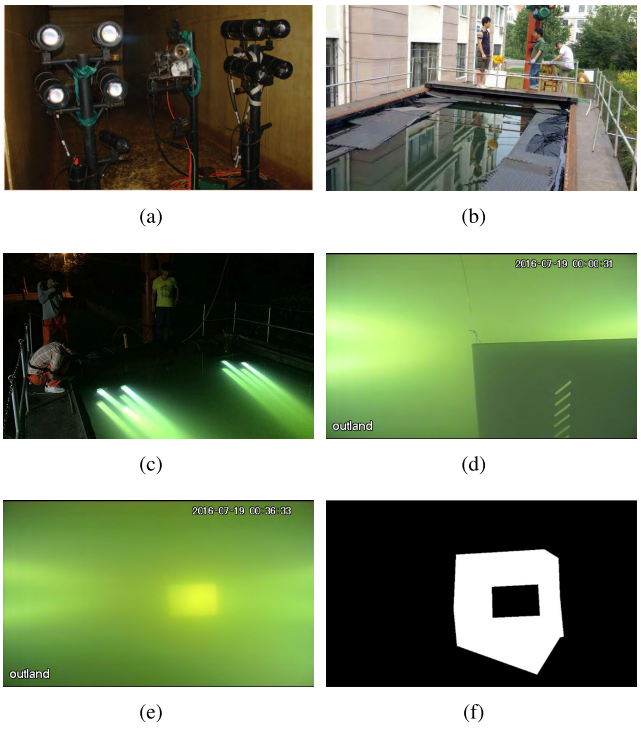

FIGURE 5. The entity of our UWLLF system (a) and experimental environment (b) and (c). (d) is an image with negative contrast near the CCD (0.4 m). (e) is an image with positive contrast at 3.5 m. (f) is an example of mask of (e) for the contrast calculation.

III. EXPERIMENTS, RESULTS AND DISCUSSION

Figure 5(b) and Figure 5(e) show the pool ($8\ m \times 3.6\ m \times 2\ m$) experiment. The target is a Lambert white board with dimensions of $54cm \times 45cm$ and every light source is equipped with a halogen lamp of 4000K color temperature. The optic-axis distance is set to 1.35 m, and the tilt angle relative to the CCD viewing axis is set according to the Figure 1. In the experiment, the target was moved away from the CCD, from 0.2 m to 6 m in 0.1 m interval. Additionally, the divergence angle and intensity of the light source, which are adjusted through different stops and neutral optical attenuators, respectively, are an additional two variables. The specific information of these three variables is shown in Table 3. In the experiment, more than 2000 images, each of which has different distances, light source intensities and divergence angles, are acquired. The manual segmentation of the target and the background is implemented like Figure 5(f) due to the huge amounts of data.

TABLE 3. Three variables in the experiment.

Target distance	$0.2m \sim 6m, 0.1m$ interval
Light source intensity	1%, 5.9%, 21.5%, 31.5%, 100%
Divergence angle	3.8°, 7.6°, 11.4°, 15.2°, 18.9°, 22.6°, 26.3°, 29.9°

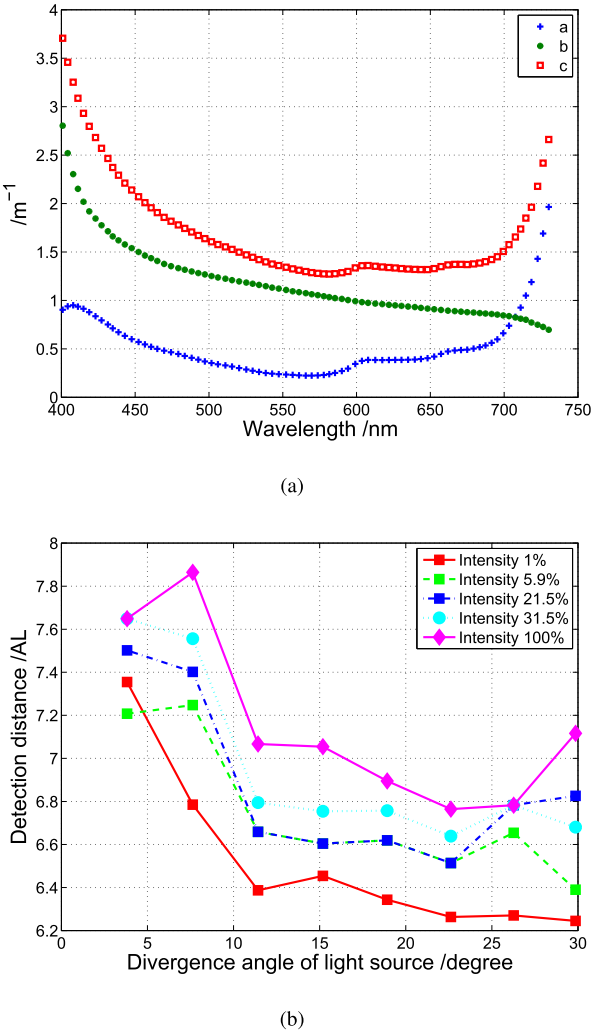

FIGURE 6. The spectral distribution of attenuation and absorption coefficients (a), and the attenuation coefficient of 532 *nm* is 1.43/*m*. (b) is the DD performance of our UEOD system.

The wavelength 532 *nm* of double YAG lasers is employed in a number of UEOD systems, such as Table 1, whose DD performance is apparently evaluated by AL (532 *nm*). Thus, for a consistent comparison of DD performance or other specifications, the attenuation length of 532 *nm* is chosen as the standard unit. As shown in Figure 6(a), the spectral distribution of attenuation and the absorption coefficients were acquired by AC-S211 of Wetlab. The attenuation coefficient of 532 *nm* is $1.43/m$, i.e., one AL is equal to 0.7 m.

As shown in the simulation of Figure 4, the DD performance of a UEOD system is related to the intensity and divergence angle of the light source. The DD performance of our UEOD system with different intensities and divergence angles is tested in the pool experiment, as shown in Figure 6(b). It reveals the downtrend of DD with increasing divergence angle. For the same intensity curve, the DD gap between the maximum and minimum is more than 1 AL; for the same divergence angle, different curves show the

DD performance VS intensity: 100% intensity leads to the largest DD, approximately 7.9 AL at 7.6° divergence angle, whereas 1% intensity only supports 6.8 AL. In other words, the DD decreases as the divergence angle increases, and the DD increases as the intensity increases. This experimental result is consistent with the preceding simulation model. In addition, the selected 100% intensity and 7.6° divergence angle in the simulation can optimize this UEOD system to a DD of 7.9 AL in the experiment.

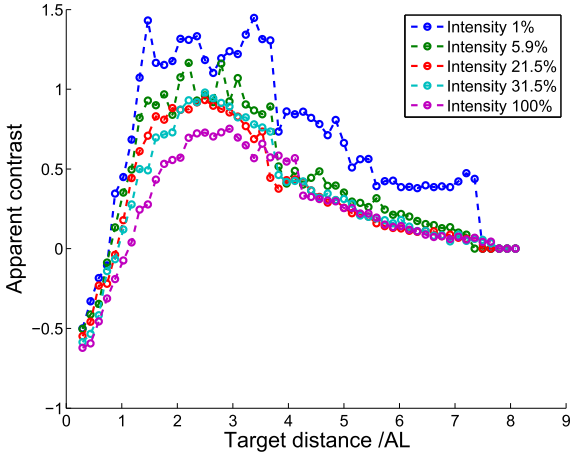

(a)

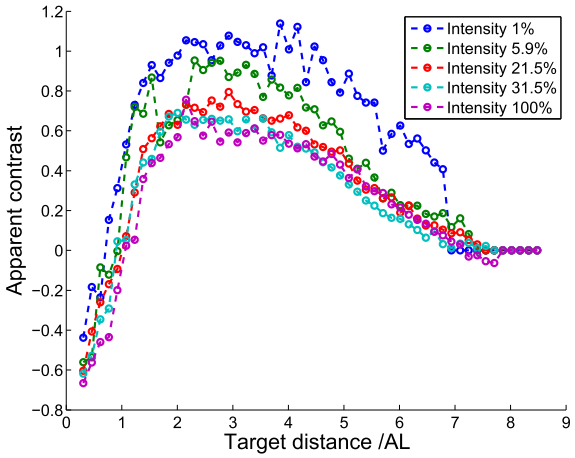

(b)

FIGURE 7. Contrast performance at divergence angles of 11.4° (a) and 29.9° (b) in the near area (LICF and LCLF levels, <5.25 AL).

A large DD is desirable, so we designed the BLLS and the light field as above. Additionally, another specification of this system is still in our consideration – contrast performance in near area (LILF and HCLF). As described in section II-B, LILF and HCLF are established in our previous work. Thus, what is the detection performance after adding the RDLF to the whole light field? Figure 7 and Figure 8 illustrate the apparent contrast of the target in LILF and HCLF levels. The apparent contrast is calculated following the principle of Equation 7, and the mask as in Figure 5(d) is used to calculate

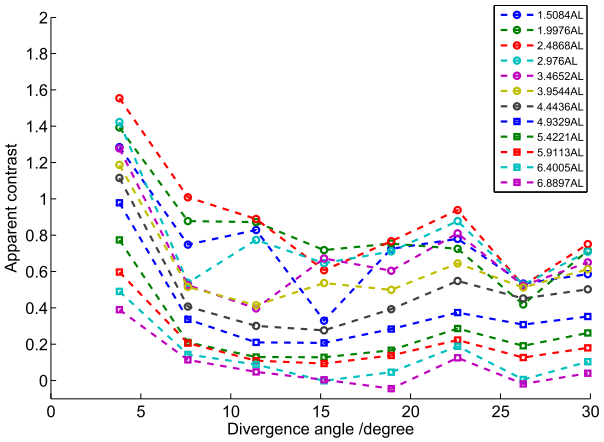

FIGURE 8. Contrast performance VS different divergence angles in the near area (LICF and LCLF levels, <5.25 AL)).

the luminance of the target and background. As shown in Figure 7 and Figure 8, there are three characteristics reflected:

- With increasing light intensity, the apparent contrast in the near area is decreasing. This is a contrary conclusion to the DD VS light intensity.
- There is negative contrast within approximately 0.8 AL, which corresponds to the images of the dark target and bright background as in Figure 5(f). This is related to the DOF discussed in the next paragraph. Strong contrast exists between 1.5 AL and 5 AL, where the target shows a sharp edge as in Figure 5(c).
- There is a slight downtrend of apparent contrast as the divergence angle increases, as shown in Figure 8. As the distance increases, the downward trend is not obvious, but it tends to be flat.

Therefore, it can be concluded that a high light intensity weakens the apparent contrast in the near area, whereas the impact of the divergence angle is slight. Overall, however, the weakened contrast is strong enough for target detection.

As shown in Figure 9, two strips with a 0.1 *m* white-black interval are used to calculate the DOF and FOV of our UEOD system. The image of the white-black strip in Figure 9(a) stretches from the nearest to the maximum detection distance. Moreover, the contrast distribution in Figure 7 demonstrates that there is no contrast data located below the threshold within the maximum DD. Additionally, negative contrast exists within approximately 0.8 AL (no-imaging zone, but still detectable). In other words, this UEOD system achieves the full DOF for underwater detection. The FOV is calculated with the same method of a white-black strip placed at 2.4 *m* from the CCD. The diagonal FOV of 67° is obtained through the triangulation calculation. Additionally, in another experimental environment (swimming pool), as shown in Figure 9(c), the large DOF and wide FOV are verified: the swim-lane of the float ball and black line are imaged from the nearest area of the horizon to the distance; thus, an almost full

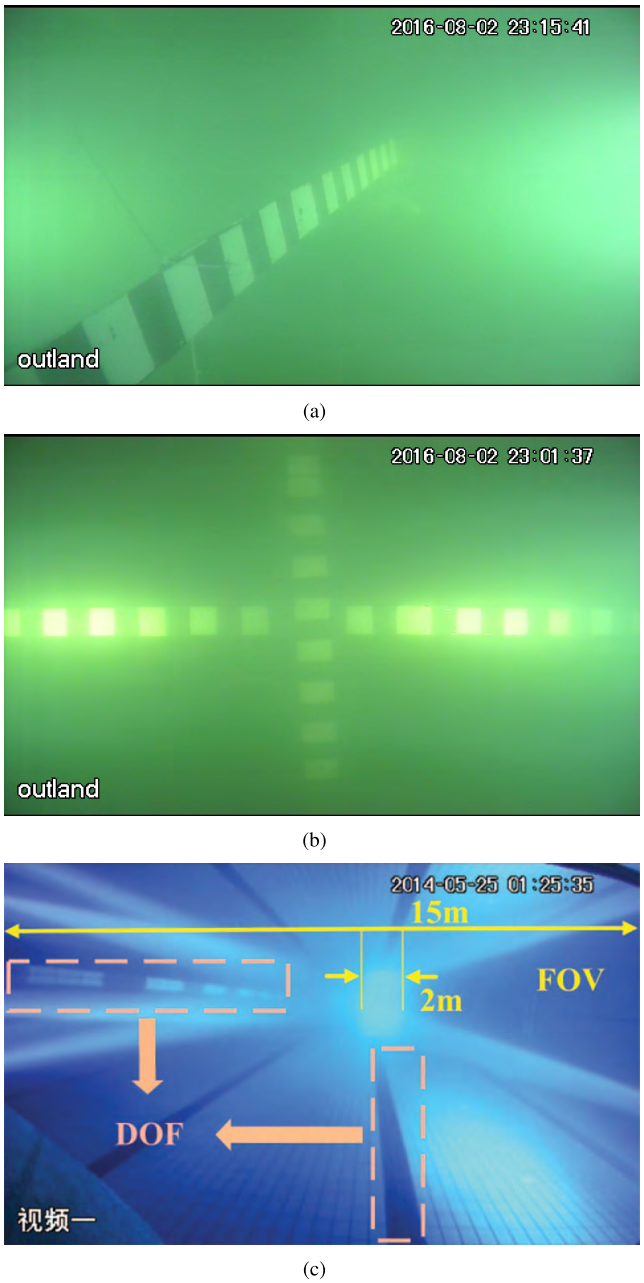

FIGURE 9. Illustration of the FOV and DOF of our UEOD system. (a) is for the DOF evaluation, imaging the white-black strip with a 0.1 *m* interval. (b) is acquired at a distance of 2.4 *m* for the FOV calculation and evaluation. (c) is acquired in another environment of water quality (13.5 *m* visibility) at a distance of 20.5 *m*, assisting in calculating the FOV and DOF.

DOF is evident. This image is acquired at 20.5 *m*; therefore, an approximate FOV of 70° is acquired.

In summary, equipped with 100% intensity and 7.6° divergence angle of the light source, this UWLLF system optimizes the underwater detection within 7.9 AL at an almost full DOF without sacrificing the FOV (70°).

IV. CONCLUSION

In conclusion, this paper presents the underwater wide-area layered light field (UWLLF). Along the detection direction, the layered structure of UWLLF in the distribution of light energy can optimize the DD of a UEOD system. Additionally, with emphasis on the UWLLF methodology, this model is tested through a pool experiment, achieving the design goal of a 70° FOV and 7 AL DD (actually up to 7.9 AL). In particular, the non-detection zone at lower energy levels is eliminated. These three improvements enhance the capability of the UEOD system in target detection, allowing it to see farther, deeper and wider. This paper only focuses on improving the image quality in the detection process, and in future work, 5 dimensions of the light field will be employed to describe the scattering characteristics of UWLLF, pursing a more precise description of energy distribution and a basis of image post-processing on removing backscattering and forescattering.

APPENDIX

To assist for the reading, the abbreviations in the paper are summarized in Table 4.

TABLE 4. The abbreviations in the paper.

DD	detection distance
FOV	field of view
DOF	depth of field
AL	attenuation length
UEOD	underwater electro-optic detection
LLS	line laser scanning
LRG	laser range gating
OPI	optical polarization imaging
STIL	streak tube image lidar
MLI	modulation light imaging
SLI	structured light imaging
UWLLF	underwater wide-area layered light field
LILF	low-energy inhomogeneous light field
HCLF	high-energy collimated light field
RDLF	remote diffuse light field
PPLF	pulse power light field
BLF	beyond light field

REFERENCES

[1] J. T. Cobb, K. C. Slatton, and G. J. Dobeck, "A parametric model for characterizing seabed textures in synthetic aperture sonar images," *IEEE J. Ocean. Eng.*, vol. 35, no. 2, pp. 250–266, Apr. 2010.
[2] F. M. Caimi, D. M. Kocak, F. Dalgleish, and J. Watson, "Underwater imaging and optics: Recent advances," in *Proc. IEEE OCEANS*, Quebec City, QC, Canada, Sep. 2008, pp. 1–9.
[3] D. M. Kocak, F. R. Dalgleish, F. M. Caimi, and Y. Y. Schechner, "A focus on recent developments and trends in underwater imaging," *Mar. Technol. Soc. J.*, vol. 42, no. 1, pp. 52–67, 2008.
[4] J. S. Jaffe, "Underwater optical imaging: The past, the present, and the prospects," *IEEE J. Ocean. Eng.*, vol. 40, no. 3, pp. 683–700, Jul. 2015.
[5] H. Sun, D. C. Hendry, M. A. Player, and J. Watson, "*In situ* underwater electronic holographic camera for studies of plankton," *IEEE J. Ocean. Eng.*, vol. 32, no. 2, pp. 373–382, Apr. 2007.

[6] A. Bodenmann, B. Thornton, and T. Ura, "Development of long range color imaging for wide area 3D reconstructions of the seafloor," in *Proc. IEEE Int. Underwater Technol. Symp.*, Tokyo, Japan, Mar. 2013, pp. 1–5.
[7] D. Alley, B. Cochenour, and L. Mullen, "Multistatic optical imaging system compatible with AUV platforms," in *Proc. OCEANS MTS/IEEE Washington*, Washington, DC, USA, Oct. 2015, pp. 1–4.
[8] H. Kondo, T. Maki, T. Ura, Y. Nose, T. Sakamaki, and M. Inaishi, "Relative navigation of an AUV using a light-section ranging system," in *Proc. IEEE ICARCV*, Kunming, China, Dec. 2004, pp. 425–430.
[9] H. Lu, Y. Li, Y. Zhang, M. Chen, S. Serikawa, and H. Kim, "Underwater optical image processing: A comprehensive review," *Mobile Netw. Appl.*, vol. 22, no. 6, pp. 1204–1211, 2017.
[10] S. Q. Duntley, "Light in the sea," *J. Opt. Soc. Amer.*, vol. 53, no. 2, pp. 214–233, 1963.
[11] C. D. Mobley, *Light and Water: Radiative Transfer in Natural Waters*, 2nd ed. New York, NY, USA: Academic, 1994.
[12] A. Gordon, "Turbid test results of the SM2000 laser line scan system and low light level underwater camera tests," *Underwater Intervent.*, vol. 94, pp. 305–311, 1994.
[13] M. P. Strand, "Underwater electro-optical system for mine identification," *Proc. SPIE*, vol. 2496, pp. 487–498, Jun. 1995.
[14] K. D. Moore, J. S. Jaffe, and B. L. Ochoa, "Development of a new underwater bathymetric laser imaging system: L-bath," *J. Atmos. Ocean. Technol.*, vol. 17, no. 8, pp. 1106–1117, 2000.
[15] G. R. Fournier, D. Bonnier, J. L. Forand, and P. W. Pace, "Range-gated underwater laser imaging system," *Opt. Eng.*, vol. 32, no. 9, pp. 2185–2191, 1993.
[16] M. P. Rowe, E. N. Pugh, J. S. Tyo, and N. Engheta, "Polarization-difference imaging: A biologically inspired technique for observation through scattering media," *Opt. Lett.*, vol. 20, no. 6, pp. 608–610, 1995.
[17] J. W. McLean and J. T. Murray, "Streak-tube lidar allows 3-D ocean surveillance," *Laser Focus World*, vol. 34, no. 1, pp. 171–176, 1998.
[18] A. Gelbart, B. C. Redman, R. S. Light, C. A. Schwartzlow, and A. J. Griffis, "Flash lidar based on multiple-slit streak tube imaging lidar," *Proc. SPIE*, vol. 4723, pp. 9–19, Jul. 2002.
[19] L. Mullen, A. Laux, B. Concannon, E. P. Zege, I. L. Katsev, and A. S. Prikhach, "Amplitude-modulated laser imager," *Appl. Opt.*, vol. 43, no. 19, pp. 3874–3892, 2004.
[20] S. G. Narasimhan, S. K. Nayar, B. Sun, and S. J. Koppal, "Structured light in scattering media," in *Proc. IEEE ICCV*, Beijing, China, vol. 1, Oct. 2005, pp. 420–427.
[21] Y. Y. Schechner and N. Karpel, "Recovery of underwater visibility and structure by polarization analysis," *IEEE J. Ocean. Eng.*, vol. 30, no. 3, pp. 570–587, Jul. 2005.
[22] B. Zheng, G. Wang, and M. Fu, "An approach for underwater target detection by inhomogeneous illumination," in *Proc. IEEE OCEANS Aberdeen*, Aberdeen, U.K., Jun. 2007, pp. 1–4.
[23] S. Q. Duntley, "Measurements of the transmission of light from an underwater source having variable beam spread," Scripps Inst. Oceanogr., Univ. California, San Diego, CA, USA, Tech. Rep. 60–57, 1960.
[24] L. E. Mertens, *In-Water Photography: Theory and Practice*, 1st ed. Hoboken, NJ, USA: Wiley, 1970.
[25] S. Q. Duntley, "The visibility of submerged objects," Scripps Inst. Oceanogr., San Diego, CA, USA, Tech. Rep., Oct. 1960.

MENGNAN SUN was born in Weihai, Shandong, China, in 1989. He received the B.S. and M.S. degrees in communication engineering and communication and information system from the Ocean University of China, Qingdao, in 2012 and 2015, respectively, where he is currently pursuing the Ph.D. degree in computer system architecture. His research interests include underwater vision, underwater scattering for imaging, and underwater light field.

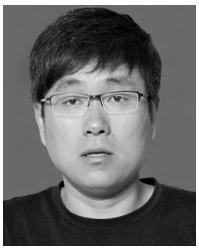

ZHAORUI GU received the B.S. and M.S. degrees from the Ocean University of China, Qingdao, China. He is currently an Experimentalist at the Department of Electronic Engineering, Ocean University of China. His research interests include image processing and underwater vision.

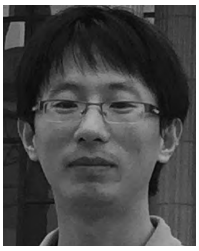

HAIYONG ZHENG received the B.S. degree in electronic information engineering and the Ph.D. degree in ocean information sensing and processing from the Ocean University of China, Qingdao, China, in 2004 and 2009, respectively.

In 2009, he joined the Department of Electronic Engineering, Ocean University of China, where he is currently an Associate Professor. His research interests include image processing, computer vision, and machine learning.

BING ZHENG received the B.S. degree in electronics and information system, the M.S. degree in marine physics, and the Ph.D. degree in computer application technology from the Ocean University of China, Qingdao, China, in 1991, 1995, and 2013, respectively.

He is currently a Professor with the Department of Electronic Engineering, Ocean University of China. His research interests include ocean optics, underwater imaging, and optical detection.

JOHN WATSON received the Ph.D. degree from the University of St Andrews in 1976, with a focus on laser microspectral analysis of steel. After five years as a Higher Scientific Officer with the U.K. Atomic Energy Authority, Caithness, U.K., in 1981, he returned to the academic world at RGIT, Aberdeen. He moved to the School of Engineering at the University of Aberdeen, in 1984, where he became a Professor of optical engineering in 2004 and the Chair of electrical engineering in 2007.

His research work has focused on the applications of lasers and optics in subsea science and engineering. His group has developed and deployed two subsea holographic cameras for the analysis of plankton and other marine particles. Other work has included subsea laser welding, laser breakdown spectroscopy, optical image processing, and color holography.